RSC Advances

PAPER

View Article Online
View Journal | View Issue

Cite this: *RSC Adv.*, 2025, **15**, 40574

Graphene instead of graphite doping potassium ferrate for intrinsically reforming both conductivity and stability of super-iron(VI) battery

Jing Dong,[ab] Dengyu Yu,[a] Di Gu,[b] Lingyue Zhu,[b] Meng Wang,[a] Dandan Yuan,[b] Hong Jiang[b] and Baohui Wang *[a]

Graphene possesses an intrinsic electronic structure and electrochemical properties that theoretically compensate for the low conductivity and poor stability of ferrate(VI) salts. A graphene coating strategy is proposed to replace graphite conductive additives, intrinsically enhancing both the conductivity and stability of potassium ferrate(VI) for battery applications. The intrinsic modification of ferrates using graphene or graphene oxide (GO) yields materials termed graphene-modified ferrates or GO-modified ferrates. Graphene's exceptional electrical conductivity significantly improves the electrical properties of ferrate(VI) battery materials. Carbon atoms in graphene provide lone-pair electrons that coordinate with ferrates, forming an electron-coordination composite structure. This interaction alleviates the electron deficiency associated with iron(VI) in these materials, facilitating improved charge transfer and contributing to enhanced overall battery performance. Electrochemical evaluations demonstrate that the hydrolysis stability of coated potassium ferrate is significantly influenced by both the coating type and the applied heat treatment. Notably, the graphene-modified ferrate(VI) battery exhibits an extended discharge duration, characterized by a prolonged time for the voltage to decrease to 0.7 V, achieving a discharge efficiency of 49%. Furthermore, the graphene coating optimizes charge transfer, culminating in a discharge efficiency of up to 82%. These findings provide robust evidence for advancing electrode materials in super-iron battery applications.

Received 22nd August 2025
Accepted 19th October 2025

DOI: 10.1039/d5ra06254c

rsc.li/rsc-advances

Introduction

In 1999, Licht *et al.* (including co-author Wang) patented a novel battery system employing Fe(VI)-valence ferrates as cathode materials, termed the "Super-Iron Battery".[1] This technology harnesses the environmentally benign nature of Fe(VI) salts coupled with their capacity for 3-electron transfer per iron center, offering significant potential for high-energy-density and sustainable energy storage solutions.[2–4] Two decades of intensive global research have focused on enhancing ferrate stability, enabling practical demonstration of ferrate battery performance. Key strategies include increased solution alkalinity,[5–8] additive ions,[9,10] and surface modifications.[11–20] However, two fundamental challenges persist: the poor conductivity of Super-Iron Battery[21,22] and their inherent thermodynamic instability.[10,23] Addressing these limitations remains critical for achieving commercially viable ferrate-based batteries. While conventional coatings such as SiO_2/TiO_2 or Y_2O_3–ZrO_2 composites mainly enhance chemical stability,[12,15,16,18] and conductive additives like Magnéli-phase titanium oxides aim to improve bulk electrode conductivity,[22] our graphene-coating strategy uniquely addresses both issues simultaneously. The graphene overlayer serves as a dense protective barrier while its high electronic conductivity and potential coordination with the Fe(VI) centers intrinsically enhance the charge transfer capability of the active material. This is reflected in the high discharge efficiency of achieved in this work, positioning it competitively among leading ferrate enhancement approaches, such as the catalytic use of CuO/RuO_2 additives.[20]

Graphene's two-dimensional lattice structure facilitates a continuous, dense coating that serves as an effective physical barrier for core materials, surpassing conventional carbons like carbon black and CNTs.[24–27] Its high in-plane charge carrier mobility and chemical stability[28–30] establish an efficient conductive network, while inherent flexibility accommodates volume variation. These properties synergistically enhance both aqueous stability and electrochemical performance in composites, demonstrating graphene's promise as a conductive scaffold for applications such as supercapacitors.[27] Recent studies on transition metal oxide/graphene composites such as $Sr_2Ni_2O_5$/rGO[31] and $BaCoO_3$/rGO[32] demonstrate enhanced capacitance, cycling stability, and energy density, providing a direct precedent

[a]*College of Chemistry and Chemical Engineering, Northeast Petroleum University, Daqing 163318, China. E-mail: wangbh@nepu.edu.cn*
[b]*College of New Energy and Materials, Northeast Petroleum University, Daqing, 163318, China*

for graphene–ferrate integration. Beyond electrode materials, interface and electrolyte engineering also play critical roles; for instance, gel polymer electrolytes have been shown to effectively reduce interfacial impedance and enhance ionic conductivity in sodium-ion batteries.[33,34] Furthermore, graphene-based designs in battery systems improve interfacial stability and ion transport,[35,36] suggesting that a graphene modification layer can simultaneously enhance both the electronic conduction and interfacial durability of K_2FeO_4.

Motivated by these prospects, this study investigating graphene (G) and graphene oxide (GO) as intrinsic modification materials for potassium ferrate (K_2FeO_4). We systematically optimized the modification conditions and developed a K_2FeO_4 electrode material with improved electrochemical performance and material stability. The modified composites were comprehensively characterized using scanning electron microscopy (SEM), linear sweep voltammetry (LSV), electrochemical impedance spectroscopy (EIS), and constant-resistance discharge testing. Our results demonstrate the significant efficacy of graphene-based coatings in improving the overall electrochemical behavior and stability of potassium ferrate. This advancement highlights the strong potential of graphene-modified K_2FeO_4 as a high-performance cathode material, particularly for next-generation super-iron batteries.

Materials and methods

Materials of experimental

Potassium ferrate(VI) (K_2FeO_4, analytical grade), graphite powder (99.95% metal basis), and L-ascorbic acid (≥99.7%) were purchased from Shanghai Macklin Biochemical Co., Ltd, Aladdin Reagent (Shanghai) Co., Ltd, and Tianjin Jinbei Fine Chemical Co., Ltd, respectively. CR2032 coin cells were obtained from Xinghua Benoit Battery Materials Co., Ltd.

Preparation of G-modified ferrates

The composite was prepared by first reducing graphene oxide (GO) to graphene (G). Briefly, 8 mg of GO (equivalent to 5 mg G after reduction) was dispersed in anhydrous ethanol and chemically reduced by adding 80 mg of L-ascorbic acid with stirring at 60 °C for 30 minutes. The resulting graphene was collected by suction filtration and purified by stirring in 30 wt% H_2O_2 to remove excess ascorbic acid, followed by a second filtration and washing. This purified graphene was redispersed, mixed with 100 mg of K_2FeO_4, and briefly stirred. The final graphene-coated potassium ferrate composite was obtained after suction filtration, vacuum-drying, and a post heat treatment at 150 °C. The materials used include unmodified pristine potassium ferrate (K), as well as two carbon-modified potassium ferrate samples: one modified with graphene oxide (GOK) and the other modified with graphene (GK), to facilitate differentiation and comparison.

Characterization

Water stability test. 100 mg of potassium ferrate material was immersed in 100 mL of distilled water under static conditions (no stirring), and the solution pH was monitored over time.

Electrode fabrication and battery assembly. The cathode was prepared by mixing 60 mg of K_2FeO_4 powder (unmodified or GO-modified) with 12 mg of acetylene black. A slurry was formed using *n*-hexane as the solvent, coated onto a 2 cm × 2 cm nickel foam substrate, and compressed with a second nickel foam piece. The electrode sheet was vacuum-dried at 35 °C for 5 h and cold-pressed at 20 MPa for 1 min to enhance mechanical stability. A zinc sheet (6 cm × 4 cm for primary cells; 0.5 cm × 0.5 cm for coin cells) served as the anode. Batteries were assembled using the prepared electrodes and a 10 mol per L KOH electrolyte.

Electrochemical performance testing. Constant-resistance discharge was performed using a 200-Ω resistor, with cell voltage recorded at 10-second intervals *via* a multimeter (VC86E). Electrochemical impedance spectroscopy (EIS) and linear sweep voltammetry (LSV) were conducted on a CHI650E electrochemical workstation. EIS measurements employed a 5 mV AC amplitude over 0.01 Hz to 100 kHz at a discharge potential of 1.5 V. LSV was performed in 10 mol per L KOH at a scan rate of 1 mV s^{-1}, using a zinc sheet as both reference and counter electrode. Data were processed using ZsimDemo and ZView software.

Results and discussion

Mechanism of graphene coating stabilization of potassium ferrate

As a representative first-row transition metal, iron adopts a high oxidation state in the FeO_4^{2-} anion, enabling its function as a potent oxidant. The inherent instability of ferrates arises from their partially filled d-orbitals, which readily accept electrons through hybridization to attain greater stability. In alkaline aqueous media, FeO_4^{2-} ions may exhibit electron deficiencies, specifically vacancies (holes), contributing to their instability. Electronically, the Fe(VI) center in FeO_4^{2-} possesses six valence electrons, typically forming two double bonds and two single bonds with oxygen atoms. Protonation in aqueous solution induces elongation of Fe–O bonds and shortening of adjacent bonds, lowering the energy of the lowest unoccupied molecular orbital (LUMO). This structural change further destabilizes the ion. Consequently, the instability of FeO_4^{2-} can be ascribed to electron holes localized on the iron centers.

In graphene, each carbon atom utilizes three of its four valence electrons in sp^2 hybridization to form three σ-bonds (bond angle ≈ 120°) with neighboring atoms. The remaining 2p electron contributes to a delocalized π-bond system extending across the basal plane, perpendicular to the σ-bond network. Intralayer C–C bonds are nonpolar covalent with a length of 142 pm, while interlayer interactions are dominated by van der Waals forces and π–π stacking.

The mechanism of electron equilibrium and transfer between graphene and ferrate is illustrated in Fig. 1 Within the G-modified ferrate composite, carbon atoms in the graphene lattice facilitate the donation of delocalized π-electrons (characterized by weaker bonding) to the FeO_4^{2-} ions. This electron

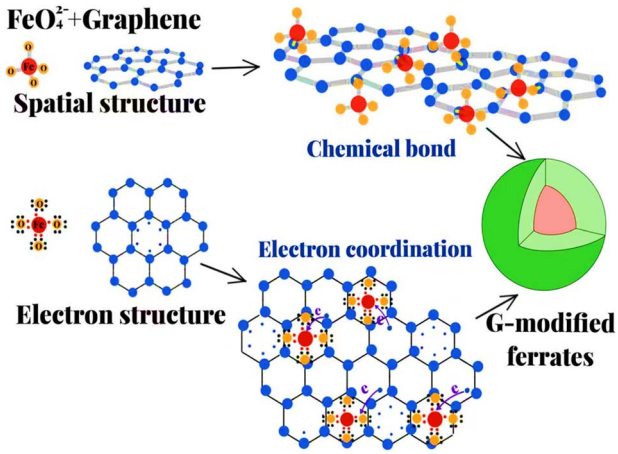

Fig. 1 Stability mechanism *via* electron balance and transfer in G-modified ferrates.

transfer fills the electron holes (vacancies) localized on the iron centers. Consequently, the electronic structure of the ferrate is optimized, and an electron-coordination composite forms between graphene and ferrate. This mechanism significantly improves the composite cathode material's electronic structure. Mitigation of the Fe atoms' electron deficiencies enhances both the material's stability and its electrochemical performance.

Characterization of the G-modified ferrates

Fig. 2a and b show unmodified potassium ferrate (K_2FeO_4) crystals exhibiting a relatively smooth surface and well-defined crystalline morphology, characterized by a plate-like structure. In contrast, Fig. 2c and d depict the graphene-modified ferrate(VI) and GO-modified ferrate(VI), respectively, revealing surfaces densely covered with numerous platelet-like particles.

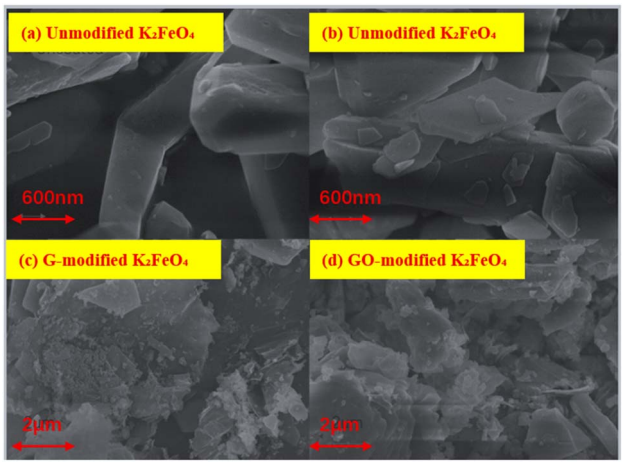

Fig. 2 Scanning electron microscopy (SEM) images of unmodified and graphene (G)-modified K_2FeO_4 particles. (a) Unmodified K_2FeO_4 at 5000× magnification (scale bar: 2 μm). (b) Unmodified K_2FeO_4 at 10 000× magnification (scale bar: 2 μm). (c) G-modified K_2FeO_4 at 5000× magnification (scale bar: 2 μm). (d) Graphene oxide (GO)-modified K_2FeO_4 at 20 000× magnification (scale bar: 2 μm).

This coating results in a roughened texture and increased particle size, attributable to the successful encapsulation of K_2FeO_4 by graphene, confirming the effectiveness of the coating process.

Following confirmation of successful graphene coating *via* SEM, further investigations are warranted to elucidate material properties and application potential. First, assessing the aqueous stability of K_2FeO_4 before and after coating is essential, as it critically impacts performance under humid conditions. Second, comprehensive evaluation of its electrochemical performance in batteries, specifically charge-discharge efficiency, is necessary to gauge its enhanced functionality.

Stability assessment of potassium ferrate in water

This study assessed the stability of K_2FeO_4 by monitoring the dynamic behavior of ferrate ions in solution and evaluating the influence of heat treatment. The hydrolysis reaction is described by:

$$2FeO_4^{2-} + 5H_2O \rightarrow 2Fe^{3+} + \frac{3}{2}O_2 + 10OH^-$$

This process significantly alters solution pH. Real-time pH monitoring enabled the construction of curves depicting temporal pH changes, reflecting the hydrolysis kinetics of K_2FeO_4 under different conditions.

The curves (Fig. 3) indicate that the pH of the solution containing graphene-modified ferrates (GK) remained more stable during the initial 20 minutes. Although graphene is inherently hydrophilic, the hydrolysis rate increased after 20 minutes, likely due to water absorption causing coating swelling, cracking, and rupture. Conversely, the GO coating (GO) did not inhibit hydrolysis and appeared to promote decomposition, attributable to the water absorption and colloidal behavior of both GO and graphene.

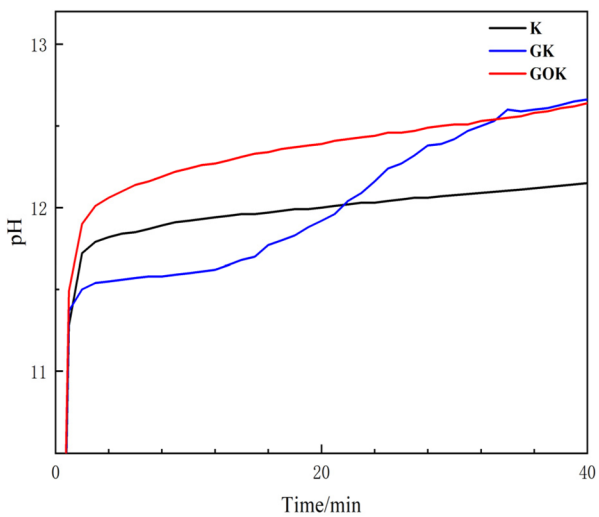

Fig. 3 pH changes during decomposition of unmodified and coated K_2FeO_4 in water (K: unmodified K_2FeO_4; GK: graphene-modified K_2FeO_4; GO: GO-modified K_2FeO_4).

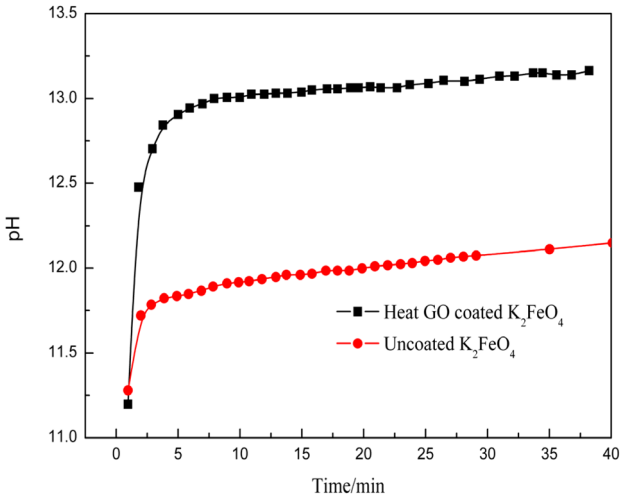

Fig. 4 pH changes during decomposition of heat-treated GO coated and unmodified K_2FeO_4 in water.

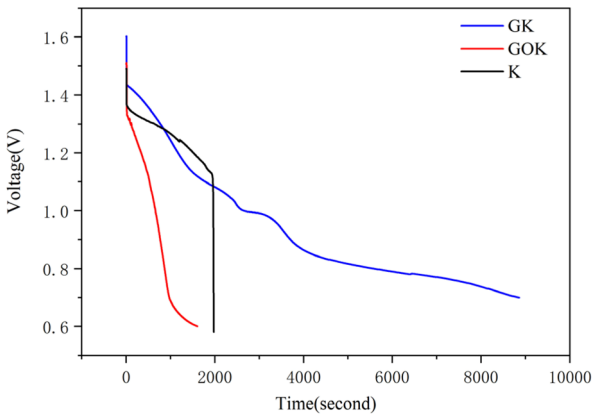

Fig. 5 Constant resistance discharge curves (200 Ω load) for coin cells with cathodes of: graphene-modified K_2FeO_4 (GK), GO-modified K_2FeO_4 (GOK), and unmodified K_2FeO_4 (K).

To investigate thermal stability relevant to applications (*e.g.*, battery discharge, high-temperature wastewater treatment), the impact of heat treatment on coated materials was examined. Fig. 4 shows the pH changes for heat-treated K_2FeO_4. The results indicate significantly reduced aqueous stability for the GO-modified ferrates material after heat treatment. This decrease may stem from:[1] the 150 °C heat treatment temperature[37] potentially being suboptimal for complete GO-to-graphene conversion, resulting in residual colloidal particles that increase the K_2FeO_4–water contact area;[2] partial decomposition of K_2FeO_4 and destabilization of its crystal structure induced by heat treatment, accelerating hydrolysis.

Graphene demonstrates potential for enhancing the short-term aqueous stability of ferrate at lower temperatures. However, the extent to which this improved solution stability translates to enhanced battery performance metrics, such as energy density, requires further investigation. Comprehensive research is essential to determine if the observed stabilization benefits the electrochemical performance of ferrate cathode materials in battery applications.

Constant resistance discharge of modified button cells

To evaluate the impact of coating strategies on the electrochemical performance and stability of potassium ferrate (K_2FeO_4), constant resistance discharge testing was performed on coin cells.

The discharge curves (Fig. 5) reveal that the cell utilizing GO-modified ferrates (GOK) exhibited a rapid voltage decline to 0.7 V within a short duration, corresponding to a low discharge capacity (approximately 9% relative to theoretical). In contrast, the cell with graphene-modified K_2FeO_4 (GK) demonstrated sustained discharge; the time to reach 0.7 V was significantly extended, yielding a higher discharge capacity (~49% relative to theoretical). The unmodified K_2FeO_4 cell (K) exhibited intermediate performance (~15% relative capacity).

These results highlight the significant advantage of the graphene modified strategy in enhancing K_2FeO_4 cathode discharge performance compared to unmodified and GO-modified ferrates. The poor performance of the GO-modified ferrates cell is attributed to the low electrical conductivity of graphene oxide and its strong hydrophilicity. Water absorption accelerates electrode material decomposition, leading to rapid capacity fade, confirming graphene oxide's unsuitability as a K_2FeO_4 coating material.

The unmodified K_2FeO_4 cell exhibited a sharp voltage drop around 2000 seconds. This may be linked to incomplete utilization of K_2FeO_4 and the formation of an iron hydroxide ($Fe(OH)_3$) passivation layer resulting from K_2FeO_4 decomposition. This layer likely facilitates further self-decomposition and impedes ionic/electronic conduction, hindering discharge. Conversely, the graphene-modified ferrates cell maintained a stable discharge profile. The graphene coating may segregate K_2FeO_4 particles, potentially localizing the effects of decomposition products (like $Fe(OH)_3$) within coated units, minimizing broader electrode degradation. Furthermore, the limited electrolyte volume in coin cells likely reduced water ingress and coating rupture, enabling robust discharge performance.

The constant resistance discharge results correlate with the aqueous stability findings: the graphene (G) coating significantly enhances K_2FeO_4 stability and discharge capacity, demonstrating its superiority as a coating material over graphene oxide (GO), which exhibits poor aqueous stability and yields limited discharge capacity in cells.

Electrochemical impedance spectroscopy (EIS) analysis

EIS is a crucial electrochemical technique that employs alternating current impedance spectra to construct physical models of coated materials and investigate structural and performance changes. Analysis of the impedance spectra yields key parameters, such as charge transfer resistance (R_{ct}) and diffusion coefficients (D), enabling objective evaluation of coating performance. This method elucidates the frequency-dependent response characteristics of electrode materials and guides performance optimization, providing significant support for developing Super-Iron battery electrodes.

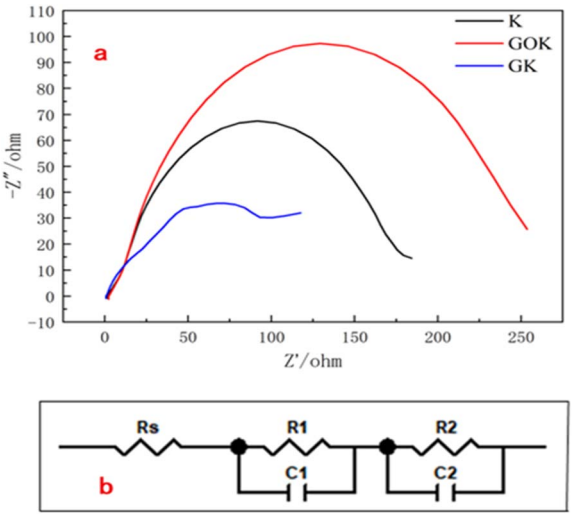

Fig. 6 (a) Electrochemical impedance spectroscopy (EIS) curves for unmodified (K), GO-modified ferrates (GOK), and graphene-modified ferrates (GK) K_2FeO_4; (b) simulated equivalent circuit diagram.

Fig. 6b illustrates the equivalent circuit. R_s represents the ohmic impedance (solution resistance), determined by the high-frequency intercept on the real axis, primarily reflecting electrolyte impedance. The electrode material's rough, porous structure enhances its capacitive behavior.

The high-frequency capacitive loop is attributed to the parallel combination of contact capacitance (C_1) and contact resistance (R_1/R_c) between K_2FeO_4 and graphene. This loop signifies the electrode's high-frequency electrochemical response. The medium-to-low-frequency loop arises from the parallel combination of the double-layer capacitance (C_2) and charge transfer resistance (R_2/R_{ct}), reflecting the charge transfer kinetics.

Analysis of Fig. 6a reveals that graphene-modified K_2FeO_4 (GK) exhibits the smallest charge transfer resistance (R_{ct}). The high-frequency region shows distorted, non-ideal semicircular behavior, characteristic of distributed surface properties or inhomogeneities potentially related to the contact capacitance (C_1). Minimizing the effective electrode area could potentially mitigate such dispersion effects.

Furthermore, Fig. 6a indicates a near-horizontal line in the low-frequency region for both unmodified K_2FeO_4 (K) and graphene-modified ferrates (GK) K_2FeO_4, absent in the GO-modified ferrates (GOK) sample. This low-frequency tail typically represents Warburg diffusion impedance. A slope approaching zero (indicating a phase angle near $-90°$) suggests diffusion-limited behavior, with the line length reflecting the magnitude of the diffusion impedance (Z_w). For unmodified K_2FeO_4, the iron hydroxide ($Fe(OH)_3$) passivation layer formed during decomposition hinders electrolyte penetration, increasing Z_w. For graphene-modified ferrates, the graphene coating initially restricts electrolyte access to the K_2FeO_4 surface, potentially leading to localized concentration depletion and elevated Z_w. Conversely, the absence of a distinct Warburg tail for GO-modified ferrates suggests graphene oxide dissolution forms a colloidal structure, facilitating unrestricted electrolyte contact and rapid charge transfer kinetics that match the decomposition rate.

In conclusion, graphene-coated K_2FeO_4 exhibits significantly lower overall impedance compared to the unmodified material, while the GO-modified ferrates demonstrates higher impedance. This disparity is primarily attributed to the substantial difference in electrical conductivity between graphene and graphene oxide. Consequently, the graphene-coated K_2FeO_4 demonstrates superior electrochemical performance relative to its GO-modified ferrates.

Constant-resistance discharge analysis of primary batteries

Constant-resistance discharge testing of primary batteries provides an advanced electrochemical assessment by simulating the discharge process. This method critically evaluates electrode materials, highlighting the significant influence of electrolyte composition on key parameters like material properties, surface characteristics, and electrode geometry. It is essential for analyzing core performance indicators, including long-term stability and discharge capacity.

Fig. 7 compares the discharge performance of K_2FeO_4 cathodes with different coatings. Quantitative analysis reveals the following discharge capacities (relative to theoretical): the GO-modified ferrates cathode achieved ~33%, the graphene modified ferrates cathode achieved ~82%, and the unmodified K_2FeO_4 cathode achieved ~39%. These results underscore the substantial advantage of the graphene coating for enhancing K_2FeO_4 discharge capacity and highlight the limitations of the graphene oxide coating.

Closer examination of Fig. 7 shows that within the initial 1300 seconds, the GO-modified ferrates cathode exhibited greater stability than the unmodified cathode. However, as discharge progressed, the unmodified cathode performance gradually surpassed that of GO-modified ferrates. This behavior is attributed to the strong hydrophilicity of the graphene oxide coating, causing water absorption from the electrolyte. This likely led to GO dissolution/swelling, forming a colloidal

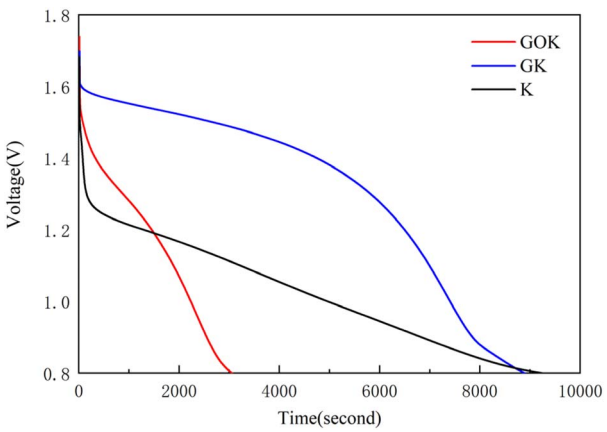

Fig. 7 Constant-resistance discharge curves for primary batteries with cathodes of: GO-modified (GOK), graphene modified (GK), and unmodified (K) K_2FeO_4 in 10 mol per L KOH electrolyte.

structure, increasing interfacial gaps, and promoting detachment of K_2FeO_4 particles from the electrode surface, culminating in a rapid voltage drop.

In contrast, the graphene modified ferrates cathode demonstrated remarkable stability throughout discharge. This stability arises from the graphene coating's ability to maintain structural integrity upon electrolyte contact (due to its mechanical strength and lower solubility in alkaline electrolyte), effectively mitigating water absorption and coating rupture. Consequently, the graphene modified K_2FeO_4 cathode exhibits excellent electrochemical performance and long-term stability in the primary battery configuration.

Linear sweep voltammetry (LSV) analysis

Linear sweep voltammetry (LSV) is a powerful electrochemical technique for probing electrode reaction mechanisms across a wide potential range. Given the effectiveness of the graphene coating demonstrated in prior electrochemical testing, LSV was performed on a primary battery utilizing graphene-coated potassium ferrate (K_2FeO_4). While the voltammetric behavior of low-valent iron species (Fe^{3+}/Fe^{2+}) is well-established, the reduction mechanism from high-valent Fe(VI) remains less explored. LSV also offers predictive insights into potential changes in coated electrode materials during electrochemical processes.

The LSV curve (Fig. 8) exhibits a prominent cathodic peak at 0.142 V, corresponding to the primary reduction of K_2FeO_4. A weaker cathodic peak observed at 0.270 V may indicate an initial single-electron reduction step (Fe(VI) → Fe(V)). Notably, the graphene-coated K_2FeO_4 cathode exhibits a significantly higher cathodic peak current density compared to unmodified K_2FeO_4 reported in ref. 17. Furthermore, its primary reduction peak potential (0.142 V) shows a less negative shift relative to the unmodified material.

This positive shift in peak potential (less negative value) suggests enhanced reaction kinetics. It can be attributed to the graphene coating's high electrical conductivity facilitating faster electron transfer and potentially improved electrolyte access to the active material. The resulting increase in local OH^- ion concentration near the electrode surface, governed by the Nernst equation, contributes to the observed shift towards a more positive potential.

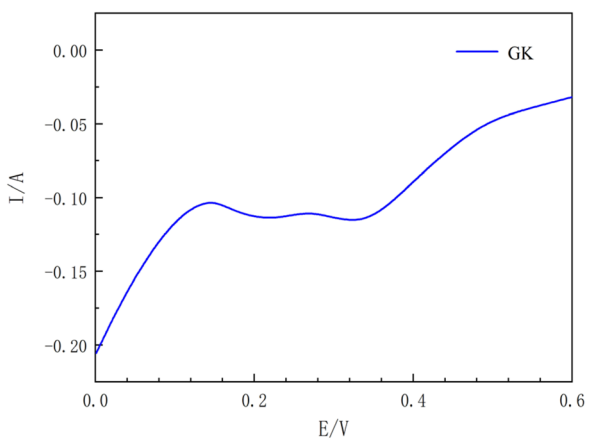

Fig. 8 Linear sweep voltammetry (LSV) curve for a primary battery with a graphene-coated K_2FeO_4 cathode (scan rate: 1 mV s^{-1}; electrolyte: 10 mol per L KOH).

While this work establishes the superior stability and discharge capacity of graphene-coated K_2FeO_4 in a primary battery configuration, future research will focus on its application in rechargeable systems. In such studies, a comprehensive analysis including full galvanostatic charge–discharge cycling, coulombic efficiency, and capacity retention over hundreds of cycles will be essential and will be thoroughly investigated.

Conclusions

This study investigated the effects of graphene coating on potassium ferrate(VI), focusing on enhancing the conductivity and stability of ferrate(VI)-based batteries. Scanning electron microscopy (SEM) confirmed the successful deposition of graphene and graphene oxide (GO) coatings. The graphene-modified ferrate(VI) exhibited a significantly extended discharge duration, achieving a discharge efficiency of 49%, compared to 15% for unmodified ferrate(VI) and 9% for GO-modified ferrate(VI). Electrochemical impedance spectroscopy further demonstrated that graphene-modified ferrate(VI) possessed the lowest charge transfer impedance. This superior charge transfer capability resulted in a significantly improved discharge efficiency of 82%, in contrast to 39% for unmodified samples and 33% for GO-modified samples. Additionally, the graphene coating significantly enhanced long-term stability, outperforming GO-modified ferrate(VI), which exhibited degradation due to water absorption. These findings underscore the substantial potential of graphene modification to markedly improve the electrochemical performance of super-iron batteries.

Author contributions

Conceptualization, J. D. and D. Yu; methodology, L. Z.; formal analysis, D. Yu; investigation, M. W.; resources, Dandan Yuan; data curation, H. J.; writing – original draft preparation, J. D.; writing – review and editing, B. W.; funding acquisition, D. G. All authors have read and agreed to the published version of the manuscript.

Conflicts of interest

There are no conflicts to declare.

Data availability

All data generated or analyzed during this study are included in this article.

Supplementary information is available. See DOI: **https://doi.org/10.1039/d5ra06254c**.

Acknowledgements

This work was supported by the National Natural Science Foundation of China (Grant No. U24B6004 and 21808030), the Natural Science Foundation of Heilongjiang Province (Grant No. LH2022B006), and the Postdoctoral Scientific Research Developmental Fund of Heilongjiang Province (Grant No. LBH-Q21082). Support was also received from the Foundation of Northeast Petroleum University (Grant No. 13051202201 and 2021YDL-06). The authors gratefully acknowledge these funding bodies for their financial support.

Notes and references

1 S. Licht, B. Wang and S. Ghosh, *Science*, 1999, **285**, 1039–1042.
2 S. Licht, B. Wang, S. Ghosh, *et al.*, *Electrochem. Commun.*, 1999, **1**, 522–526.
3 S. Licht, B. Wang, G. Xu, *et al.*, *Electrochem. Commun.*, 1999, **1**, 527–531.
4 S. Licht, V. Naschitz, L. Bing, *et al.*, *J. Power Sources*, 2001, **99**, 7–14.
5 K. A. Walz, A. N. Suyama, W. E. Suyama, *et al.*, *J. Power Sources*, 2004, **134**, 318–323.
6 Z. Xu, J. Wang, H. Shao, *et al.*, *Electrochem. Commun.*, 2007, **9**, 371–377.
7 W. Yang, J. Wang, T. Pan, *et al.*, *Electrochim. Acta*, 2004, **49**, 3455–3461.
8 V. K. Sharma, S. Tala, V. Bláha *et al.*, in *Ferrites and Ferrates: Chemistry and Applications in Sustainable Energy and Environmental Remediation*, American Chemical Society, Washington, DC, USA, 2016, pp. 241–253.
9 M. Kolar, P. Novak, K. Machalova, *et al.*, *Phys. Chem. Chem. Phys.*, 2016, **18**, 4415–4422.
10 B. Wang, J. Dong, D. Gu, *et al.*, *Ionics*, 2016, **22**, 1967–1972.
11 J. Huang, Z. Yang, S. Wang, *et al.*, *J. Solid State Electrochem.*, 2015, **19**, 723–730.
12 K. A. Walz, J. R. Szczech, A. N. Suyama, *et al.*, *J. Electrochem. Soc.*, 2006, **153**, A1102–A1107.
13 B. Yang, Z. Yang, S. Wang, *et al.*, *J. Electroanal. Chem.*, 2012, **687**, 3–10.
14 S. Wang, Z. Yang, D. Liu, *et al.*, *Electrochem. Commun.*, 2010, **12**, 367–370.
15 Y. Zhang, G. Zhang and T. Du, *Electrochim. Acta*, 2011, **56**, 1159–1163.
16 Y. Zhang, X. Zhao, S. Zhang, *et al.*, *Appl. Energy*, 2012, **99**, 265–271.
17 H. Chen, Z. Yang, R. Wen, *et al.*, *Electrochim. Acta*, 2012, **75**, 62–70.
18 X. Yu and S. Licht, *J. Power Sources*, 2007, **173**, 1012–1016.
19 K. A. Walz, A. Handrick, J. R. Szczech, *et al.*, *J. Power Sources*, 2007, **167**, 545–549.
20 S. H. Ye, Y. Y. Wang, Q. L. Sun, *et al.*, *Electrochim. Acta*, 2011, **56**, 4691–4695.
21 S. Licht, X. Yu and D. Zheng, *Chem. Commun.*, 2006, 4341–4343.
22 M. V. Simičić, M. I. Čekerevac, L. N. Nikolić-Bujanović, *et al.*, *Electrochim. Acta*, 2017, **247**, 516–523.
23 C. Yan, L. Zhu, J. Dong, *et al.*, *R. Soc. Open Sci.*, 2019, **6**, 180919.
24 F. Bonaccorso, Z. Sun, T. Hasan, *et al.*, *Nat. Photonics*, 2010, **4**, 611–622.
25 R. Rinaldo, V. Alberto, P. Stefano, *et al.*, *Nat. Mater.*, 2015, **14**, 271–279.
26 Z. J. Fan, J. Yan, L. J. Zhi, *et al.*, *Adv. Mater.*, 2010, **22**, 3723–3728.
27 F. Ahmad, M. Zahid, H. Jamil, *et al.*, *J. Energy Storage*, 2023, **72**, 108731.
28 Z. S. Wu, W. Ren, L. Xu, *et al.*, *ACS Nano*, 2011, **5**, 5463–5471.
29 S. Kumar, S. Pal, V. Kumar, *et al.*, *Luminescence*, 2022, **38**, 909–953.
30 M. Navarro-Rodriguez, V. Camús, A. Cros, *et al.*, *Appl. Surf. Sci.*, 2024, **642**, 158611.
31 F. Ahmad, M. A. Khan, U. Waqas, *et al.*, *RSC Adv.*, 2023, **13**, 25316–25326.
32 M. Shahzada, F. Ahmad, M. Ibraheem, *et al.*, *RSC Adv.*, 2025, **15**, 6308–6323.
33 A. Iqbal, R. Nadeem, A. Shakoor, *et al.*, *J. Energy Storage*, 2025, **134**, 118207.
34 F. Ahmad, A. Shahzad, S. Sarwar, *et al.*, *J. Power Sources*, 2024, **619**, 235221.
35 M. Bai, M. Zhong, W. Shen, *et al.*, *Mater. Chem. A*, 2025, **13**, 8865–8875.
36 M. Zhong, M. Bai, W. Shen, *et al.*, *ACS Appl. Mater. Interfaces*, 2024, **16**, 5813–5822.
37 Y. Shang, T. Li, H. Li, *et al.*, *Compos. Part B*, 2016, **99**, 106–111.